JOURNAL OF AGRICULTURAL AND FOOD CHEMISTRY

Open Access

pubs.acs.org/JAFC

Article

Molecular Insights into Soy Protein−Lupin Flour Meat Analogues through FTIR Spectrochemical Analysis

Aayushi Kadam, Matias Rodriguez Elhordoy, Daniel Vazquez, Alejandra Medrano, Kathleen M. Gough,* and Filiz Koksel*

Cite This: J. Agric. Food Chem. 2026, 74, 5616−5626

Read Online

ACCESS | Metrics & More | Article Recommendations | Supporting Information

ABSTRACT: Fourier transform infrared (FTIR) spectroscopy and spectrochemical imaging were used to investigate the structural and compositional changes in extruded high-moisture meat analogues (HMMAs) produced from soy protein isolate and lupin flour (LF) blends. Extrusion induced shifts in the amide I band (~1637 cm^{-1} in raw blends to ~1650 cm^{-1} in HMMAs), indicating protein denaturation and structural rearrangement associated with fibrous structure formation. Changes in carbohydrate- and lipid-associated bands further reflected extrusion-driven molecular reorganization. FTIR spectrochemical analysis revealed distinct HMMA regions, including aligned protein-rich domains and lipid−starch-rich domains appearing as polygonal grids. Increasing the LF content from 15 to 45% progressively increased lipid- and carbohydrate-associated spectral features (i.e., areas of the fatty acid ester peak at 1744 cm^{-1} and the carbohydrate peak around 1060 cm^{-1}) relative to proteins. These insights advance the understanding of structure−function relationships in HMMAs and highlight the value of FTIR spectrochemical imaging for optimizing texture and the effective design of meat analogues.

KEYWORDS: *FTIR spectroscopy, spectrochemical imaging, starch−protein interactions, extrusion cooking, texture*

1. INTRODUCTION

High-moisture meat analogs (HMMAs) are designed to mimic the texture and sensory characteristics of ground and whole meat products. Mouthfeel and texture of these products play pivotal roles in their consumer acceptance.[1,2] By closely mimicking the fibrous and/or layered structure of animal meat, plant-based HMMAs can offer a more authentic mouthfeel and eating experience compared to traditional plant-based products like tofu, tempeh, and seitan.

Understanding the structural characteristics of meat analogs is crucial for optimizing both sensory and nutritional composition. Microstructure directly affects texture, appearance, and overall palatability, while distribution and organization of macronutrients within the food matrix influence nutritional aspects, including digestion, absorption, and bioavailability.[3] Structural analysis helps manufacturers optimize processing conditions to achieve the desired product characteristics. Knowledge of how ingredients and processing conditions (e.g., temperature, shear, and moisture content) affect the retention and distribution of nutrients (proteins, lipids, and vitamins) can guide the formulation of meat analogs tailored to meet specific dietary requirements or preferences, such as low-fat or high-protein options. Overall, a comprehensive understanding of HMMA structure is essential for improving product quality and market acceptance of these plant-based meat alternatives.[4]

Many methods are employed to characterize the fibrous structure of meat analogues, including visual observation, microscopy (scanning electron microscopy, light microscopy and confocal scanning laser microscopy), X-ray tomography, and spectroscopy.[5,6] Among these, Fourier transform infrared (FTIR) spectroscopy has emerged as a powerful tool for analyzing the composition of HMMAs as well as the macronutrient interactions within HMMAs.[7] Infrared light triggers molecular vibrations inherently distinctive to various functional groups; FTIR spectroscopy provides qualitative and quantitative information about the chemical bonds and overall composition of a material. In the FTIR spectrum, each component is defined by a distinct set of characteristic absorption bands that correspond to specific molecular vibrational modes such as bond stretching or angle bending within the functional groups. These absorption bands can overlap, but the presence of several signature key bands serves to identify individual components. Bondu et al., 2024,[7] reviewed the role of FTIR spectroscopy in examining the secondary structural changes in plant proteins subjected to high-moisture extrusion cooking. They highlighted how variations in sample preparation, spectral analysis, and data interpretation, particularly peak deconvolution and reference databases, can lead to inconsistencies in the results across studies.

FTIR spectrochemical imaging combines spatial resolution on the order of 5 μm with the chemical analysis of infrared spectroscopy, allowing precise mapping of component distribution at the micrometer scale.[8,9] The spatial resolution

Received: August 12, 2025
Revised: January 19, 2026
Accepted: January 22, 2026
Published: February 5, 2026

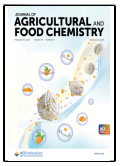

is wavelength-dependent, resulting in pixel dimensions of approximately 3 μm for CH stretching, 6 μm for the amide I band, and 10 μm for the carbonyl region. Many studies have used synchrotron radiation-FTIR (S-FTIR) microspectroscopy to raster scan across various grains and oilseeds, yielding good-quality spectra when sample preparation is correct.[8] However, restricted access (a few days) and the need for experienced personnel have reduced the applicability of S-FTIR in large-scale studies. Atomic force microscopy-coupled FTIR was used to demonstrate phase separation of lipid and protein distributions at the nanoscale in extruded peanut protein biomass waste.[10]

In this study, we have employed far field-FTIR spectrochemical imaging to investigate the microstructure and molecular composition of HMMAs made from blends of soy protein isolate (SPI) and lupin flour (LF). SPI is one of the most commonly used ingredients in HMMA production.[11] LF, being rich in dietary fiber, antioxidants, and bioactive compounds, contributes to the development of functional meat analogues while reducing reliance on highly refined ingredients.[12] The selected SPI:LF ratios ranging from 85:15 to 55:45 for HMMA production were chosen to balance the functional performance with the nutritional and sustainability goals. Gradually increasing the proportion of LF up to 45% allows evaluation of LF's impact on textural and structural integrity of HMMAs, while still ensuring sufficient protein content and processability. By analyzing frozen, thinly sectioned samples, we visualized the distribution of proteins, lipids, and carbohydrates with a high spatial resolution. To the best of our knowledge, this is the first detailed investigation using far field-FTIR spectrochemical imaging with focal plane array (FPA) detection to characterize the structural organization of HMMAs at the micron scale.

2. MATERIALS AND METHODS

2.1. Materials

SPI (SUPRO EX45) was obtained from Azelis Canada Inc. (Brampton, ON, Canada). *Lupinus angustifolius* beans were supplied by Juan Pablo Viera (Colonia, Colonia, Uruguay). These unshelled, full-fat seeds were milled at Molino Guido (Santiago Vázquez, Montevideo, Uruguay) using a Miag HN roller mill (Miag, Braunschweig, Germany) to produce LF with a particle size of less than 1 mm. The flour was further milled using a Retsch ZM200 centrifugal mill (Retsch GmbH, Haan, Germany) at 6000 rpm, with a 500 μm sieve to achieve a finer particle size. During milling, the temperature was maintained below 35 °C.

2.2. FTIR Spectroscopy Analysis of Raw Materials

FTIR spectroscopy of powdered raw materials was performed with an infrared spectrometer (INVENIO, Bruker Corporation, MA) equipped with an attenuated total reflectance accessory with diamond window (Pike Technologies, WI, USA). Spectral scans were recorded in the range of 4000−600 cm^{-1} with a wavenumber resolution of 4 cm^{-1}, accumulating 64 scans per measurement. FTIR spectra obtained were analyzed with Omnic 9.2 software (Thermo Fisher Scientific Inc., MA, USA) without any additional spectral data manipulation (no smoothing, baseline correction, etc.). All samples were analyzed in triplicate.

2.3. Preparation of HMMAs

Four blend formulations were prepared by mixing SPI and LF in ratios of 85:15 (blend 1), 75:25 (blend 2), 65:35 (blend 3), and 55:45 (blend 4). HMMAs produced by Elhordoy et al. (2025)[12] were used in this study, prepared using a lab-scale, corotating twin-screw extruder (MPF19, APV Baker Ltd., Peterborough, UK) as described by Singh et al. (2023).[13] A constant screw speed of 200 rpm, moisture content of 70% on a wet basis, and a feed rate of 0.5 kg/h on a dry basis were used. The screw profile was set following Ghanghas et al. (2024).[11] The long cooling die attached to the end of the barrel had internal dimensions of 30 cm × 5 cm × 5 mm.[14] The temperature from the feeder to the die end was set at 60−80−110−120−80−50 °C. Extrudates were collected in triplicate for each blend formula in ∼5 cm long strips of 5 cm width and 0.5 cm thickness.

2.4. Sample Preparation for IR Imaging

A subsample (0.5 cm × 0.5 cm × 0.5 cm) was cut from the center of each HMMA strip. These subsamples were immersed in an optimal cutting temperature compound (OCT; Sakura FinetekInc. Torrance, CA, USA), frozen at −80 °C and cryo-sectioned at −20 °C (Leica CM 1520, Nussloch, Germany) as shown in Figure 1. The 5 μm-thick

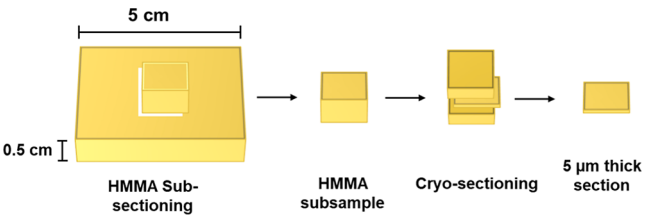

Figure 1. Preparation of thin sample sections of high-moisture meat analogue (HMMA) for FTIR spectrochemical imaging.

cryosections were collected on CaF_2 salt substrates (25 mm diameter, 1 mm thick, COE Optics) for standard transmission FTIR spectroscopic analysis.[12] These cryosections were viewed under an optical microscope at 4−40× magnification, to obtain an overview of the HMMA microstructure. Visibly different regions of the heterogeneous material were selected for FTIR spectrochemical imaging.

2.5. Far-Field IR Spectrochemical Imaging

Cryo-sectioned HMMA sections of each bend sample were imaged in transmission mode in triplicate using an Agilent Cary 670 interferometer and 620 IR microscope equipped with a 64 × 64 FPA mercury cadmium telluride detector. The IR microscope was equipped with a 15× objective and condenser with 0.62 numerical aperture and high magnification optics[9] to provide a nominal spatial resolution of 1.1 × 1.1 μm^2 per pixel. All spectra were acquired as averages of 128 scans, 4 cm^{-1} spectral resolution, ratioed against a background of 512 scans acquired on a clean region of the CaF_2 substrate. Spectral acquisition and data analysis were performed with the ResolutionsPro FTIR spectroscopy software (Ver. 5.3.01964, Agilent Technologies Inc., Santa Clara, CA, USA) following Bakir et al. (2020 and 2024).[16,17] The system was purged of CO_2 and water vapor. No baseline corrections were required; the original spectra were used directly without further manipulation. False color images to illustrate spatial distribution of components were created by integrating the area under the curve for a single marker band or by taking the ratio of the area of one marker against another.

3. RESULTS AND DISCUSSION

3.1. FTIR Spectroscopy Analysis of the Raw Materials

The FTIR spectra of the raw materials are shown in Figure 2. In contrast, LF was comprised of 35.1 ± 0.3% protein, 7.4 ± 0.2% fat, 42.3 ± 0.7% dietary fiber, and 11.7% nondietary fiber carbohydrates. Both SPI and LF exhibited protein spectral profiles with an amide I peak (mainly C═O stretch) at ∼1637 cm^{-1}. The amide II peak (C−N−H angle bend and C−N stretch) was observed at ∼1517 cm^{-1} for SPI and at 1540 cm^{-1} for LF, indicating some possible variation in their structure and composition.[15,18] All raw blends showed an amide I peak at 1637 cm^{-1} and an amide II peak at 1522 cm^{-1}. The spectral

https://doi.org/10.1021/acs.jafc.5c10733
J. Agric. Food Chem. 2026, 74, 5616−5626

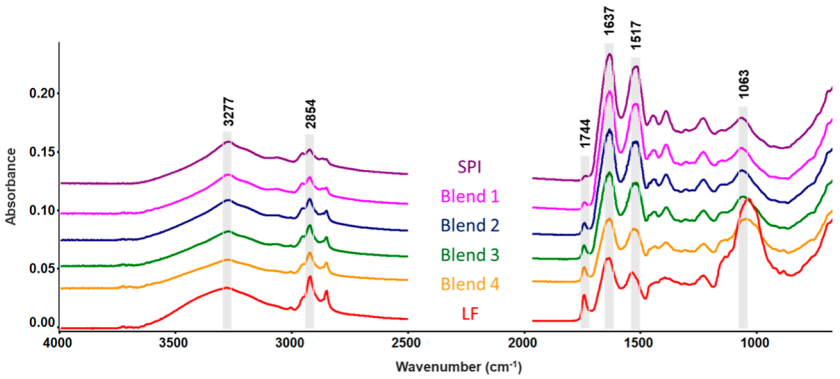

Figure 2. FTIR spectra of the raw materials. Blends (SPI:LF) are (1) 85:15; (2) 75:25; (3) 65:35 and (4) 55:45. SPI: soy protein isolate; LF: lupin flour. Spectra are displayed on a common scale, offset for clarity.

bands were assigned according to the standard literature (Table 1).

Table 1. IR Spectral Bands of the Raw Materials and High-Moisture Meat Analogues (HMMAs) by Vibrational Mode and Functional Group

peak (cm^{-1})	vibrational mode	molecular assignment[a]
3550−3100	N−H stretch of proteins and OH stretch of polysaccharides	protein, carbohydrate
2930	various CH modes	lipid, carbohydrate
2855−2852	CH_2 symmetric stretch	lipid (acyl chain)
1745−1744	C═O stretch	fatty acid ester
1700−1600	C═O stretch (amide I)	protein
1540−1515	C−N−H bend with C−N stretch (amide II)	protein
1060−1030	O−C−O modes	carbohydrate

[a]Refs 17,53−57.

SPI is primarily composed of two globulins: 7S (β-conglycinin) and 11S (glycinin). 7S globulin is a trimer consisting of α, α', and β subunits with molecular weights ranging from 52 to 72 kDa. These subunits are relatively low in cysteine, methionine, and tryptophan, leading to fewer disulfide bonds and a more flexible, less organized secondary structure.[19] This structural flexibility is reflected in the lower energy of the amide II peak of SPI at 1517 cm^{-1}, as evidenced by the shift in the amide II peak to higher wavenumbers as the SPI concentration decreases in the blends, indicative of more random coils or β-turns.[19,20] In contrast, 11S globulin, a hexamer with a molecular weight of 300−380 kDa, is composed of acidic and basic polypeptides linked by disulfide bonds, resulting in a more rigid and compact structure. The higher cysteine, methionine, and tryptophan content in glycinin contributes to a relatively more stable secondary structure.[19] This ordered structure is reflected in the sharper amide I peak at 1637 cm^{-1}, corresponding to the strong C═O vibrations typical of proteins with a high degree of structural organization.

Lupin protein is mainly composed of globulins, with a 9:1 ratio of globulins to albumins. The primary globulins in lupin are α-conglutin (legumin-like, 11S), β-conglutin (vicilin-like, 7S), γ-conglutin (7S), and δ-conglutin (2S). Of these, α-conglutin (330−440 kDa) and β-conglutin (143−260 kDa) account for about 90% of the total globulin content. The α-conglutin, similar to soy protein's 11S glycinin, is likely to form more ordered secondary structures, contributing to the presence of β-sheets and α-helices.[21] However, β-conglutin, like the 7S β-conglycinin of soy protein, has a more open and flexible structure due to fewer disulfide bonds, which could explain the slightly higher wavenumber of the amide II peak at 1540 cm^{-1} in LF, indicative of greater structural variability.[22]

The LF was rich in lipids, primarily in the form of long chain fatty acid esters (FAE), evident from the FAE C═O at 1744 cm^{-1} and appearance of the two strong CH_2 bands at 2854 and 2925 cm^{-1}, distinctive of acyl chains. A small peak at ∼3008 cm^{-1} indicates the presence of unsaturated fatty acids;[23] however, the unsaturated C═C bond is readily oxidized,[24] and the attenuation of this peak in the blends may also be due to the dilution of unsaturated fatty acids as the SPI concentration increased. These observations aligned well with the findings of Johnson et al. (2017) and Elhordoy et al. (2025)[12,25] who reported that lupin seeds have a fat content of about 6−7%, primarily in the form of triglycerides. The lipid profile includes 19% saturated fatty acids, 33% monounsaturated fatty acids, and 48% polyunsaturated fatty acids.[25]

The higher carbohydrate content of LF compared to SPI[12] was evidenced by the strong carbohydrate C−O stretching vibrations between 1150 and 950 cm^{-1}, with a local maximum at 1063 cm^{-1}. Additionally, the spectral profile in the CH stretch region, with the local maximum around 2930 cm^{-1} and absence of a symmetric CH at 2854 cm^{-1} and the broad, intense OH stretching band centered at 3287 cm^{-1}, further confirmed the presence of polysaccharides with complex overlapping spectral bands.[17,26] FTIR spectral bands at ∼1041 cm^{-1} and at ∼1400 cm^{-1} might indicate the presence of cellulose and pectin, respectively,[27,28] the two major nonstarchy polysaccharides found in lupin.[29,30]

Carbohydrate and lipid were both present, as seen in the FTIR spectrum of commercial grade SPI (Figure 2). The SPI spectrum showed a broad, characteristic carbohydrate profile with a maximum of ∼1070 cm^{-1} and a fatty acid ester carbonyl band at 1741 cm^{-1}. In comparison to the LF, the SPI had less carbohydrate and lipid, as seen by the much lower intensity of these marker bands relative to the protein amide I and II bands in SPI, versus that seen in LF.

From blend 1 to blend 4, increasing the LF concentration resulted in a gradual increase in lipid and carbohydrate content, as demonstrated by the FTIR spectra (Figure 2). The intensity of the FAE marker bands (1744 cm^{-1} and 2853 cm^{-1}) and that of the carbohydrate C−O, centered at 1063

https://doi.org/10.1021/acs.jafc.5c10733
J. Agric. Food Chem. 2026, 74, 5616−5626

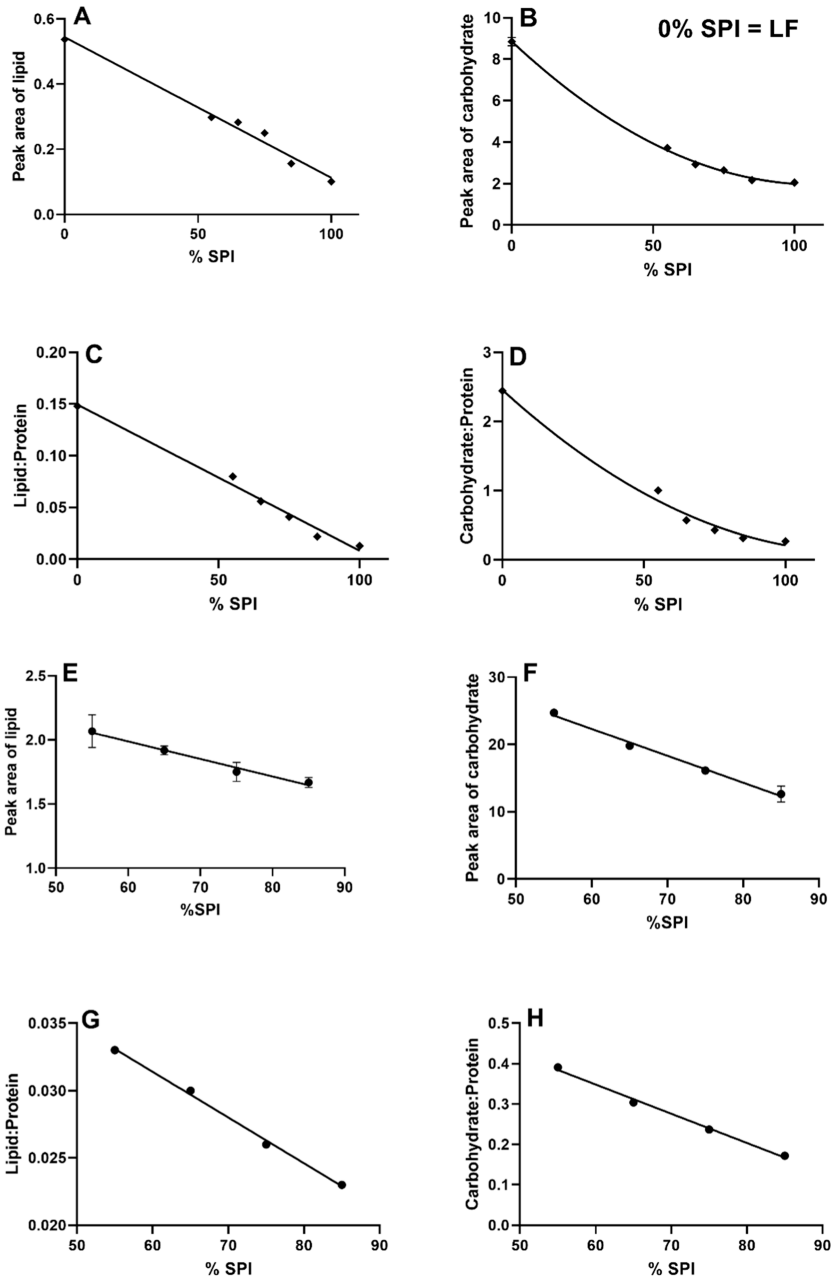

Figure 3. Integrated FTIR peak areas and area ratios as a function of soy protein isolate (SPI) concentration in the raw materials (A–D) and high-moisture meat analogues (HMMAs) (E–H). LF: Lupin flour.

cm^{-1}, illustrate the expected increase in lipid and carbohydrate contents relative to total protein (amide I and II) with the added LF.

As shown in Figure 3, the peak area of FAEs (Figure 3A) and the peak area ratio of lipid-to-protein (Figure 3C) decreased linearly with increasing SPI concentration from raw LF to LF-SPI blends to SPI (Table 2). The peak area of carbohydrates (Figure 3B) and the carbohydrate-to-protein ratio (Figure 3D) exhibited a slight deviation from a linear relationship with increasing SPI concentration, likely due to the differing carbohydrate profiles of SPI and LF.

3.2. FTIR Spectrochemical Imaging of HMMAs

Initial analysis of the cryo-sectioned HMMAs under the white light microscope showed heterogeneity at the millimeter to micrometer length scale. All HMMA sections displayed two visibly different areas under 4× magnification, labeled as regions 1 and 2 (Figure 4).

Visualization of these two distinct areas under 10× and 40× magnification showed that region 1 was a contiguous, film-like structure, while region 2 included islands in which material had formed a polygonal, frequently hexagonal grid-like network (Figure 5). Overall, the majority of the HMMA area visualized in Figure 4 was composed of the film-like structures in region 1, whereas the structures shown in region 2 were dispersed throughout the HMMA in localized pockets, which contributed to much smaller areas. These regions could result from structuring processes occurring at different length scales and times during extrusion cooking. It has been suggested that protein aggregate particles align at the nanoscale to form a protein-rich phase during HMMA structuring, while other biopolymers, such as starch, create a secondary biopolymer

https://doi.org/10.1021/acs.jafc.5c10733
J. Agric. Food Chem. 2026, 74, 5616–5626

Table 2. FTIR Peak Areas and Ratios from Specific Bands of the Raw Materials and the High-Moisture Meat Analogues (HMMAs)[a,b]

		lipid	protein	carbohydrate	ratios	
sample		C=O at 1744 cm^{-1}	amide I	region around 1060 cm^{-1}	fat/protein	carbohydrate/protein
raw materials	SPI	0.098 ± 0.005	7.515 ± 0.282	1.986 ± 0.119	0.013	0.269
	LF	0.527 ± 0.013	3.720 ± 0.102	8.973 ± 0.201	0.148	2.441
	blend 1	0.153 ± 0.005	6.997 ± 0.077	2.137 ± 0.046	0.022	0.312
	blend 2	0.247 ± 0.006	6.257 ± 0.103	2.642 ± 0.003	0.041	0.429
	blend 3	0.277 ± 0.005	5.158 ± 0.097	2.907 ± 0.039	0.054	0.564
	blend 4	0.298 ± 0.011	3.783 ± 0.084	3.736 ± 0.182	0.080	1.003
HMMA-blend 1	region 1	1.669 ± 0.039	73.460 ± 1.286	12.611 ± 1.166	0.023	0.172
	region 2-star-shaped area	2.465 ± 0.048	32.053 ± 0.048	12.091 ± 0.076	0.077	0.377
	region 2-hexagonal edge	0.601 ± 0.016	8.077 ± 0.068	27.754 ± 0.097	0.074	3.436
HMMA-blend 2	region 1	1.750 ± 0.073	67.996 ± 2.937	16.114 ± 0.178	0.026	0.237
	region 2-star-shaped area	2.280 ± 0.136	29.367 ± 0.581	18.084 ± 0.128	0.078	0.616
	region 2-hexagonal edge	0.564 ± 0.024	7.922 ± 0.070	26.485 ± 0.515	0.071	3.343
HMMA-blend 3	region 1	1.919 ± 0.034	64.978 ± 0.148	19.785 ± 0.270	0.030	0.304
	region 2-star-shaped area	1.887 ± 0.015	24.987 ± 0.212	18.048 ± 0.173	0.076	0.722
	region 2-hexagonal edge	0.591 ± 0.039	8.095 ± 0.116	26.557 ± 0.446	0.073	3.281
HMMA-blend 4	region 1	2.068 ± 0.127	63.217 ± 0.462	24.705 ± 0.270	0.033	0.391
	region 2-star-shaped area	1.947 ± 0.045	25.759 ± 0.300	19.378 ± 0.384	0.076	0.752
	region 2-hexagonal edge	0.512 ± 0.015	7.230 ± 0.185	24.850 ± 0.286	0.071	3.437

[a]For the regions 1 (the contiguous, film-like structures) and 2 (the hexagonal grid networks) of the HMMAs, refer to Figure 4. [b]SPI: Soy protein isolate, LF: Lupin flour.

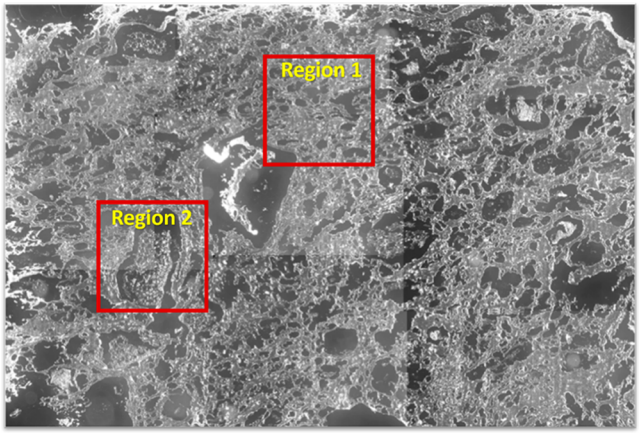

Figure 4. Optical microscope image of blend 1 high-moisture meat analogue (HMMA) section at 4× magnification illustrating heterogeneity from a contiguous film to hexagonal grids.

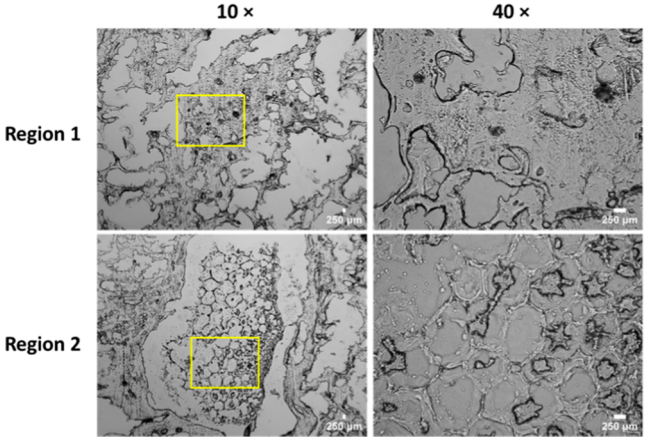

Figure 5. Optical microscopy images of regions 1 (film-like) and 2 (hexagonal grid-like) from a section of blend 1 high-moisture meat analogue (HMMA), at 10× and 40× magnification. The yellow boxes indicate the regions imaged at 40× magnification.

layer at the microscale distributed within this protein-rich phase.[31] Solidification and stabilization of the final three-dimensional (3D) network occur during the slow cooling in the cooling die. The dispersed phase, primarily consisting of protein aggregates, starch, or other fibrous materials, embeds within the continuous protein phase, giving rise to the meat-like structure in the extrudate.[31,32] Previous research by Singh et al. (2023)[13] demonstrated the heterogeneous 3D microstructure of HMMAs across top, center and bottom surfaces using X-ray microtomography.

Spectrochemical analysis within regions 1 and 2 revealed a distinct chemical heterogeneity. The grayscale micrograph and false color FTIR image of region 1 integrated on amide I are illustrated in Figure 6. The yellow box in the grayscale image (Figure 6A) delineates the area imaged. The false color image created from the integrated intensity of the amide I band across the FPA (Figure 6B) shows the distribution of components on a scale of blue (low) to red (high). Red spots had absorbance values ≫1.0 where the sample was too dense for the profile to be properly observed. Cross hairs on the false color image denote the pixel at which this spectrum was recorded. The FTIR spectrum (Figure 6C) of this contiguous, film-like region showed a predominant amide I peak at ~1650 cm^{-1}, indicating its protein richness. Both the FAE carbonyl at 1744 cm^{-1} and the carbohydrate region around 1073 cm^{-1} were present. The ratios of the peak areas for lipid/protein and carbohydrate/protein of this region were closer to that of raw SPI (Table 2). These regions represent protein-dense domains of the HMMAs.

In the context of HMMAs, the contiguous, film-like regions that are protein-rich may have formed due to the aggregation and cross-linking of proteins subjected to high temperatures and shear forces during extrusion. During the high-moisture

https://doi.org/10.1021/acs.jafc.5c10733
J. Agric. Food Chem. 2026, 74, 5616−5626

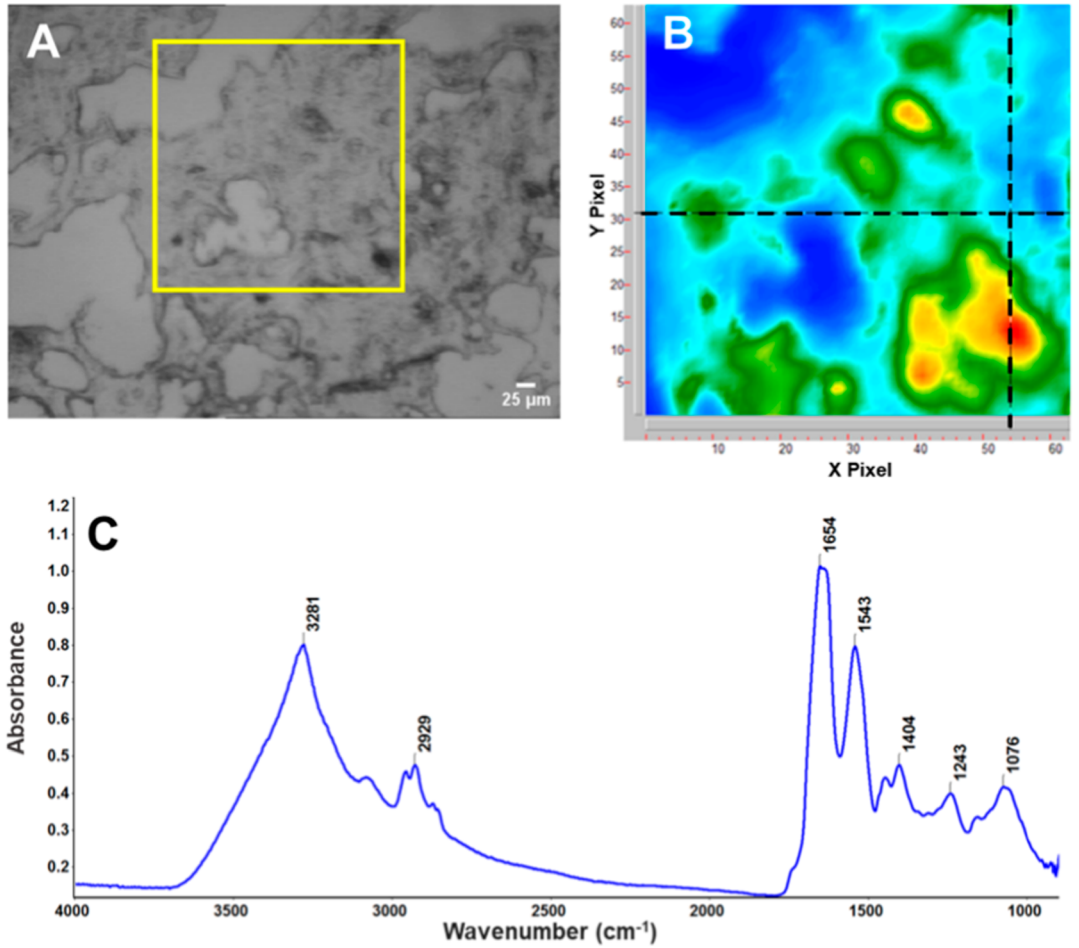

Figure 6. Far-field FTIR analysis of contiguous region 1 of blend 1 high-moisture meat analogue (HMMA). (A) Greyscale image. The yellow box delineates the area imaged. (B) False color image integrated for amide I band intensity. (C) FTIR spectrum recorded at the crosshairs in (B).

extrusion process, proteins undergo significant structural transformation due to a combination of thermal and mechanical stresses. The heat from the extruder barrel and the shearing action of the screws disrupt the natural globular structure of the proteins, leading to their denaturation.[33] This process causes a rearrangement of the protein molecules, breaking original disulfide bonds and various noncovalent interactions, such as hydrogen, ionic, and hydrophobic bonds.[34] The unfolding increases the likelihood of protein aggregation; some aggregates dissolve in water while others remain intact.[32] Toward the end of the extrusion, an elongated cooling die encourages the alignment of proteins in the flow direction, facilitating the formation of an anisotropic network. This alignment is crucial for creating the fibrous texture characteristic of HMMAs.[35,36]

The contiguous, film-like regions in HMMAs may indicate areas where proteins have aligned parallel to the shear direction. In these protein-rich regions, strong protein−protein interactions, such as disulfide bonds, hydrogen bonds, and hydrophobic interactions, could be more prevalent.[32] These interactions would stabilize the aligned protein structures, resulting in the continuity and uniformity observed in these areas. Studies suggest that the degree of these interactions can directly influence the texture and firmness of the final product.[37]

In strong contrast to the contiguous nature of region 1, the hexagonal grid-like network, i.e., region 2 in Figure 5, exhibited small, star-shaped contiguous material at the hexagonal vertices (e.g., circle in Figure 7A,B). Spectra from the star-shaped area showed strong bands at 1744, 1632, and 1072 cm^{-1}, indicating that the content of this region was rich in FAE, protein, and starch (Figure 7C). This may be due to starch−lipid and starch−lipid−protein complexes that are typically formed during extrusion processing.[38]

Starch−lipid complexes are formed when lipid molecules are encapsulated within the hydrophobic cavities of amylose single helices. These complexes are stabilized by noncovalent interactions, including hydrogen bonding, hydrophobic interactions, and van der Waals forces.[39] The $\alpha(1\rightarrow4)$ glucan helices in starch have hydrophilic hydroxyl groups on their outer surface and a hydrophobic cavity that can accommodate lipid molecules. In amylose−lipid complexes, the lipid's aliphatic chain fits into the amylose helix, while its polar groups remain outside due to steric and electrostatic effects. These complexes can organize into crystalline lamellae structures, contributing to V-type crystallinity, although the exact development of these structures is still debated.[38,40] The starch−lipid−protein complexes are thought to arise from an initial interaction between starch and lipid, followed by the association of proteins with the preformed complex.[41] The presence of FAEs in the HMMAs can facilitate the formation of ternary complexes, potentially involving three key structural elements: starch−FAE complexes, protein−FAE complexes, and disulfide-linked protein aggregates serving as a structural

https://doi.org/10.1021/acs.jafc.5c10733
J. Agric. Food Chem. 2026, 74, 5616−5626

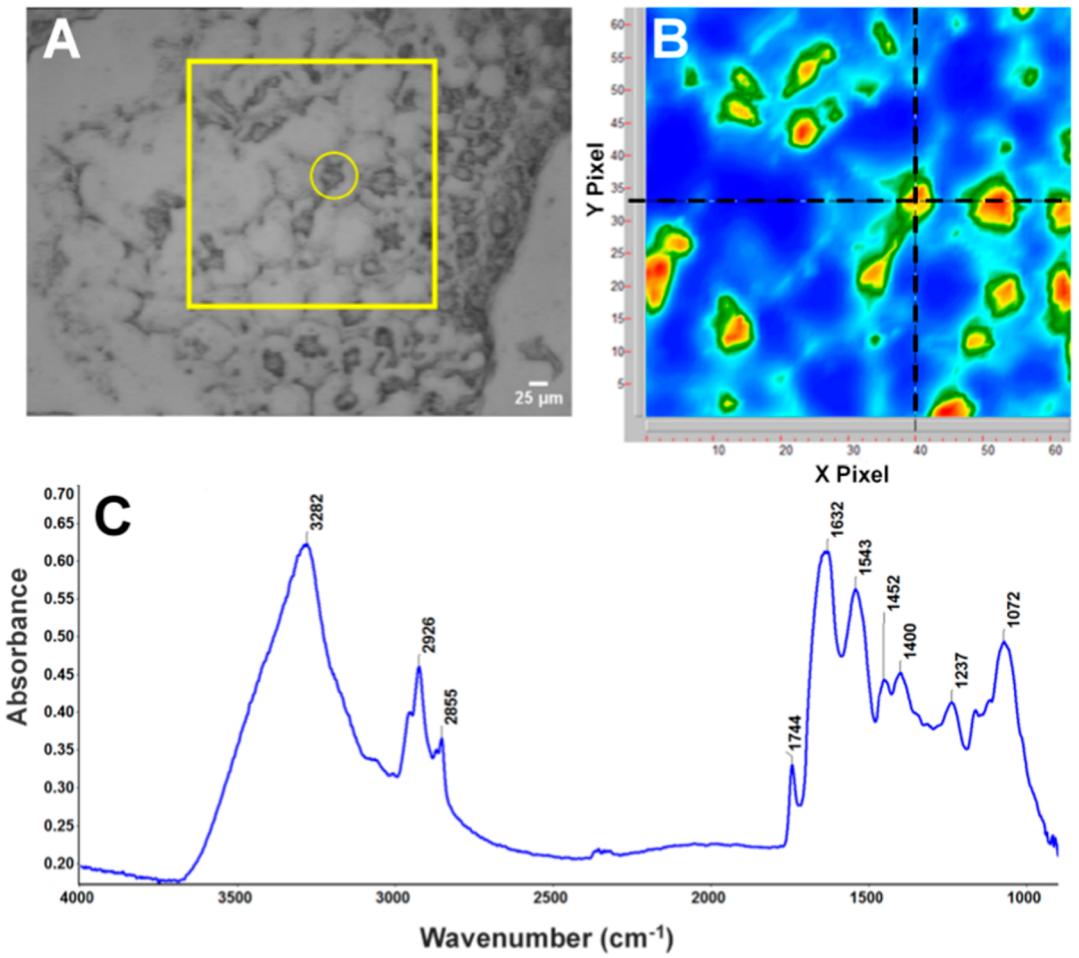

Figure 7. Far-Field FTIR analysis of the star-shaped area in region 2 of blend 1 high-moisture meat analogue (HMMA). (A) Greyscale image. The yellow box delineates the area imaged; the yellow circle shows the star-shape examined in (C). (B) False color image integrated for amide I. (C) FTIR spectrum recorded at the crosshairs in (B).

organizer.[42,43] In food processing, starch−lipid−protein complexes play a crucial role in modifying the functional properties of starch. These complexes are thought to form an insoluble film on the starch granule surface, delaying water absorption, raising the gelatinization temperature, and restricting granule swelling.[39] This film can enhance the thermal stability of starch and modify the overall pasting properties of foods. Research by Zhang and Hamaker (2003)[44] revealed that when starch, lipid, and protein were all present in a food matrix, the food's pasting profile as measured using a Rapid Visco Analyzer exhibited a distinct viscosity peak during cooling. However, this peak was absent when starch was combined with either protein or free fatty acids alone. Ultimately, starch−lipid−protein complexes forming during processing can affect the texture, shelf life, and digestibility of food products, including meat analogues.

In clear distinction to the contiguous matter, the spectrum from the hexagonal edges in region 2 (Figure 8) exhibited a very strong carbohydrate content, with the strongest carbohydrate band centered at ∼1053 cm^{-1}, as well as the typical carbohydrate CH stretch profile and broad OH stretching band at ∼3333, confirming their starch-rich nature. Both protein and lipid were much lower, as seen from the much higher carbohydrate to protein ratio and the decreased intensity of the relevant marker bands.

Starch granules, composed of amylose and amylopectin, form semicrystalline structures in their native form, with crystallinity primarily arising from amylopectin. During extrusion, the intense thermal and mechanical energy inputs, together with abundance of water, induce (partial) gelatinization, disrupting hydrogen bonds and destroying the native crystalline structure of starch granules.[45] However, as noted by Wang et al. (2018),[46] residual starch crystallinity can remain after extrusion.

Upon cooling after gelatinization, the recrystallization of amylose and amylopectin is governed by both thermodynamic and rheological factors. Thermodynamically, the system tends toward a lower-energy, more ordered state, promoting the reassociation of starch chains through hydrogen bonding. Amylopectin, in particular, has a strong tendency to form B-type crystals, which are periodically arranged in a hexagonal lattice. Amylose may also recrystallize into V-type structures—depending on its molecular interactions, for example with lipids—or into B-type crystals as affected by cooling conditions.[47−50] Rheologically, the shear applied during extrusion disentangles and aligns starch chains along the direction of flow, facilitating molecular mobility and promoting reassociation during the subsequent cooling phase in the die.[51] The combination of the thermodynamic drive for higher crystallinity and alignment of starch chains as a result of shear

https://doi.org/10.1021/acs.jafc.5c10733
J. Agric. Food Chem. 2026, 74, 5616−5626

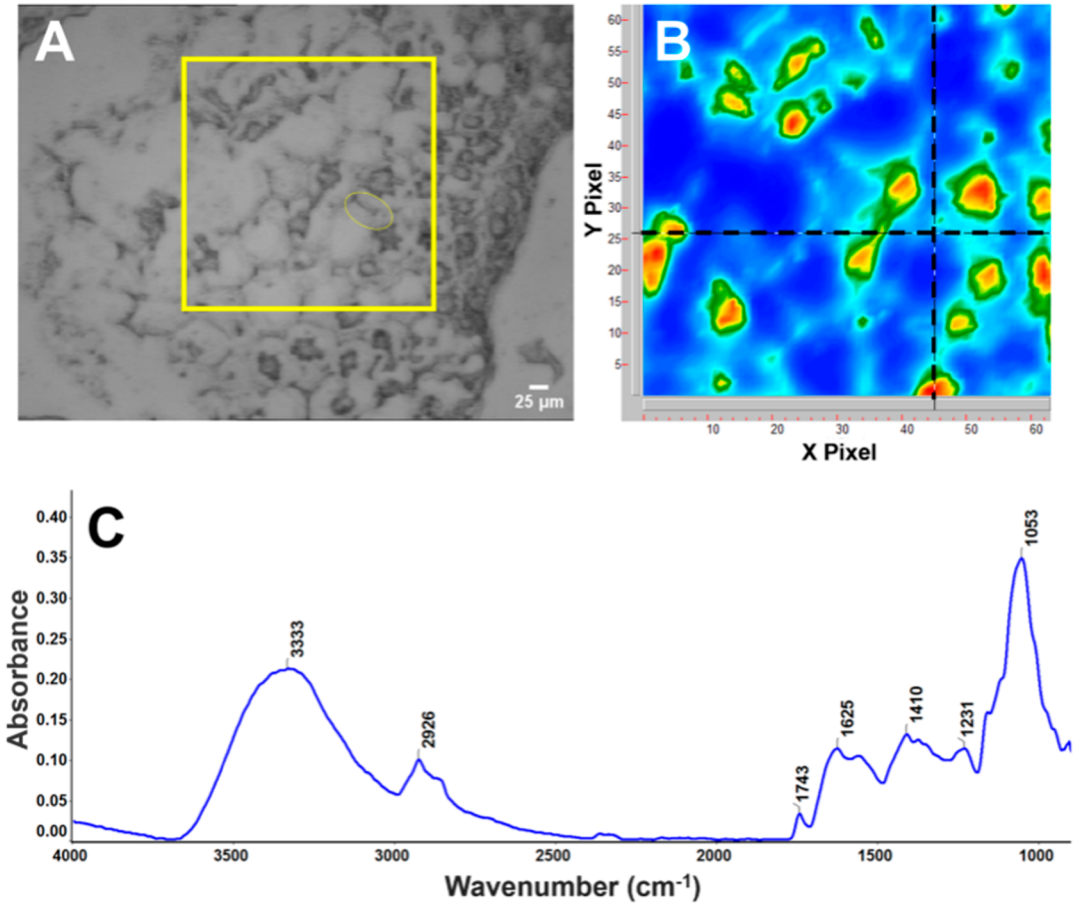

Figure 8. Far-Field FTIR analysis of the hexagonal edges in region 2 of blend 1 high-moisture meat analogue (HMMA). (A) Greyscale image. The yellow box delineates the area imaged and yellow oval shows the hexagonal edge. (B) False color image integrated for amide I band intensity. (C) FTIR spectrum recorded at the crosshairs in (B).

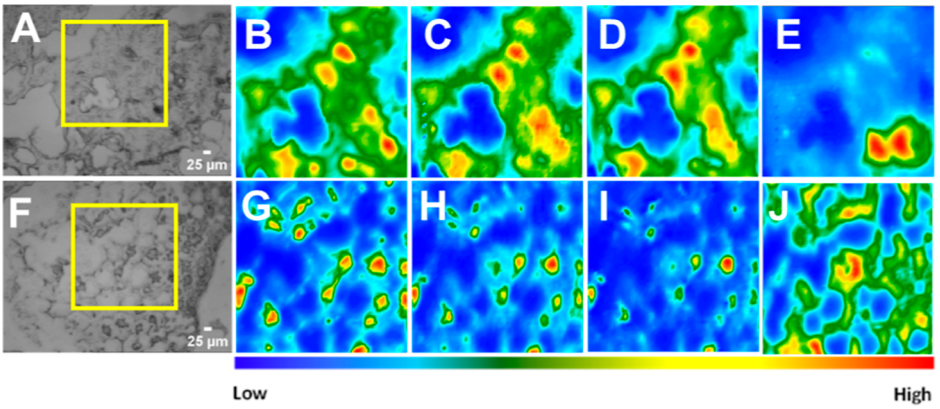

Figure 9. Distribution and localization of components in regions 1 (A–E) and 2 (F–J) of the blend 1 high-moisture meat analogue (HMMA). Greyscale micrographs (A,F). The yellow boxes delineate the areas imaged. False-color images integrated for band intensity of amide I (B,G); symmetric CH_2 (C,H); C═O stretch at 1744 cm^{-1} (D, I); carbohydrates at 1052 cm^{-1} (E, J).

likely contributes to the observed hexagonal morphology in the extruded samples.

Spectrochemical analysis of regions 1 and 2 of the HMMAs consistently showed the amide I peak maximum at ∼1637 cm^{-1}, amide II at ∼1550 cm^{-1}, carbohydrate at ∼1052 cm^{-1}, phosphate at ∼1238 cm^{-1}, lipid carbonyl at 1745 cm^{-1} and CH_2 at ∼2854 cm^{-1} (Figures 7C and 8C). The observed changes in the amide I and II peaks of the HMMAs compared to those of the raw materials provide critical insights into the structural modifications of proteins, particularly concerning denaturation and rearrangement of secondary structures. The amide I and II peaks, which are sensitive to the protein's secondary structure, showed noticeable changes in shape, position, and area after extrusion processing, indicative of the modification of the protein structure due to the combined effects of high temperature and shear forces.[7]

Since the amide I band is due to C═O stretching vibrations in the protein backbone, it is highly sensitive to the protein

https://doi.org/10.1021/acs.jafc.5c10733
J. Agric. Food Chem. 2026, 74, 5616−5626

secondary structure. The sharp amide I peak observed at ~1637 cm^{-1} (Figure 2), as noted in the raw material analysis, is commonly attributed to strong β-sheet structures (Bondu et al., 2024). The shift of amide I peak to ~1650 cm^{-1} after extrusion is indicative of protein aggregation into a predominantly helical form.[7,52] Simultaneously, the amide II peak exhibited a shift toward lower frequency after extrusion, which also indicates alterations in the protein secondary structure, further confirming the disruption of the native protein structure. The denaturation and subsequent realignment of proteins during extrusion cooking and in the long cooling die led to the formation of new structural arrangements, which could include α-helices.[52]

Brightfield and false color images of contiguous film polygonal regions in blend 1 (Figure 9) illustrate the spatial distribution of the protein, lipid, and carbohydrate. Protein and lipid are closely associated within the contiguous film region (Figure 9A–D), sharing a largely overlapping distribution pattern. The carbohydrate (Figure 9E) is concentrated on one small region; a small crystal of carbohydrate was also detected (peak at around 1052 cm^{-1}, Figure S1). The relative concentration of these components varied across the regions, indicating localized differences in their abundance. The distributions of protein, lipid, and carbohydrate were significantly different in the polygonal regions (Figure 9F–J). Protein and lipid were again colocalized, being concentrated at the vertices of the polygons in the "star-shaped" regions (Figure 9F–I). The carbohydrates were concentrated in the bars of the polygons, as seen in Figures 7 and 8. Ratios of concentrations relative to protein revealed further heterogeneity at the micrometer scale (Figure S2). When ratioed against the area of the protein band, it was discovered that there were occasionally points of very high FAE and carbohydrate colocalized, relative to much lower protein.

All HMMAs, regardless of blend formulation (blends 1 to 4), exhibited the same structural heterogeneity as observed in blend 1 HMMA, characterized by the two distinct regions. In all HMMAs, the contiguous film-like region showed an increase in the area of the FAE peak at 1744 cm^{-1} and the carbohydrate peak around 1060 cm^{-1}, along with a decrease in the amide I peak area, as the concentration of LF in the blends increased (Table 2). The edges of the hexagonal grid-like network showed similar lipid/protein and carbohydrate/protein ratios, while the star-like structures exhibited constant FAE/protein ratio, with a notable increase in the carbohydrate/protein ratio as LF concentration increased (Figure 3E–H). These changes are evidence of enhanced starch–lipid–protein complexation as lipid and carbohydrate content rises, reinforcing the concept of a dynamic interaction among these macromolecules. The increasing lipid content in the blends likely promotes the ternary complex formation, further confirming the role of FAEs in modulating starch and protein interactions.

This study provides critical insights into the structural evolution of SPI-LF HMMAs obtained through FTIR spectroscopy and spectrochemical imaging. The FTIR spectra of raw SPI and LF exhibited distinct compositional differences, with LF showing the expected higher carbohydrate and lipid contents, which would influence the formation of starch–lipid–protein complexes during extrusion. Spectrochemical imaging of fresh, desiccated thin sections illustrated the heterogeneity of the HMMA blends, showing separate protein- and starch-rich regions. The protein-rich areas occurred as contiguous, film-like structures, with spectra indicative of protein denaturation followed by reorganization. The starch-rich regions formed hexagonal networks, probably due to the crystallization of amylopectin. These results underscore the importance of protein-starch interactions and their impact on the fibrous texture of plant-based HMMAs. Notably, this study employed an innovative approach whereby FTIR spectrochemical imaging enabled a microscale examination of structural and compositional changes before and after the extrusion process. The structural organization revealed through bright-field microscopy and IR spectrochemical image analysis underscores the complexity of HMMAs. The heterogeneity discovered in HMMA sections may play an important role in mimicking the fibrous texture of animal meat since different regions would contribute to varying mechanical and sensory properties. Further research is underway to explore these possibilities. Understanding these changes in molecular distribution could aid in optimizing the formulation and processing conditions for the development of high-quality plant-based meat analogues.

■ ASSOCIATED CONTENT

Supporting Information

The Supporting Information is available free of charge at https://pubs.acs.org/doi/10.1021/acs.jafc.5c10733.

FTIR imaging and spectra of soy protein–lupin flour high-moisture meat analogues, including greyscale images, false-color chemical maps, and representative spectra highlighting carbohydrate, lipid, and protein distributions (PDF)

■ AUTHOR INFORMATION

Corresponding Authors

Kathleen M. Gough − *Department of Chemistry, Faculty of Science, University of Manitoba, Winnipeg R3T 2N2 Manitoba, Canada*; Email: kathleen.gough@umanitoba.ca

Filiz Koksel − *Department of Food and Human Nutritional Sciences, Faculty of Agricultural and Food Sciences, University of Manitoba, Winnipeg R3T 2N2 Manitoba, Canada; Richardson Centre for Food Technology and Research, University of Manitoba, Winnipeg R3T 2N2 Manitoba, Canada;* orcid.org/0000-0002-6277-4314; Email: filiz.koksel@umanitoba.ca

Authors

Aayushi Kadam − *Department of Food and Human Nutritional Sciences, Faculty of Agricultural and Food Sciences, University of Manitoba, Winnipeg R3T 2N2 Manitoba, Canada*

Matias Rodriguez Elhordoy − *Departamento de Ciencia y Tecnología de Alimentos, Facultad de Química, Universidad de la República, 11800 Montevideo, Uruguay;* orcid.org/0000-0003-1577-8707

Daniel Vazquez − *Instituto Nacional de Investigación Agropecuaria (INIA), Área Agroalimentos, Estación Experimental INIA La Estanzuela, 70006 Colonia, Uruguay*

Alejandra Medrano − *Departamento de Ciencia y Tecnología de Alimentos, Facultad de Química, Universidad de la República, 11800 Montevideo, Uruguay*

Complete contact information is available at: https://pubs.acs.org/10.1021/acs.jafc.5c10733

Notes

The authors declare no competing financial interest.

■ ACKNOWLEDGMENTS

The authors gratefully acknowledge Dr. Paul Fernyhough and Dr. Darrell Smith (Division of Neurodegenerative and Neurodevelopmental Disorders, St. Boniface Hospital Albrechtsen Research Centre) for their support. F.K. acknowledges the Discovery Grants program (RGPIN: 6037-2018) of the Natural Sciences and Engineering Research Council of Canada (NSERC), as well as Canada Foundation for Innovation (CFI), JELF program for infrastructure support. F.K. and K.M.G. acknowledge the University Collaborative Research Program of the University of Manitoba. A.M. acknowledges the financial support from the Agencia Nacional de Investigación e Innovación (ANII) MR through scholarships POS_NAC_2022_1_174183 and MOV_CA_2021_1_171688; Programa de Desarrollo de las Ciencias Básicas (PEDECIBA); and Comisión Sectorial de Investigación Científica through Project 22420230100104UD. This research was funded in part by the Governments of Canada and Manitoba under the Sustainable Canadian Agricultural Partnership, a federal - provincial - territorial initiative.

■ REFERENCES

(1) Michel, F.; Hartmann, C.; Siegrist, M. Consumers' Associations, Perceptions and Acceptance of Meat and Plant-Based Meat Alternatives. *Food Qual. Prefer.* **2021**, *87*, 104063.
(2) Weinrich, R. Opportunities for the Adoption of Health-Based Sustainable Dietary Patterns: A Review on Consumer Research of Meat Substitutes. *Sustainability* **2019**, *11* (15), 4028.
(3) Turgeon, S. L.; Rioux, L.-E. Food Matrix Impact on Macronutrients Nutritional Properties. *Food Hydrocolloids* **2011**, *25* (8), 1915−1924.
(4) Godschalk-Broers, L.; Sala, G.; Scholten, E. Meat Analogues: Relating Structure to Texture and Sensory Perception. *Foods* **2022**, *11* (15), 2227.
(5) Mota da Silva, A. M.; Lima, M. A.; Koksel, F.; Kawazoe Sato, A. C. Incorporation of Brewer's Spent Grain into Plant-based Meat Analogues: Benefits to Physical and Nutritional Quality. *Int. J. Food Sci. Technol.* **2024**, *59*, 3870−3882, DOI: 10.1111/ijfs.17134.
(6) Schlangen, M.; van der Doef, I.; van der Goot, A. J.; Clausen, M. P.; Kodger, T. E. Meat Analogues: The Relationship between Mechanical Anisotropy, Macrostructure, and Microstructure. *Curr. Res. Food Sci.* **2025**, *10*, 100980.
(7) Bondu, C.; Gimeno, F.; Evon, P.; Vaca-Medina, G.; Rouilly, A. Use of FTIR to Study Secondary Structure of Texturized Plant Proteins by High Moisture Extrusion Cooking, a Comprehensive Review. *Food Res. Int.* **2024**, *197*, 115147.
(8) Bhuiyan, Md. H. R.; Ngadi, M. O. SR-FTIR Microspectroscopy: Emerging 2D Structural-Chemical Analytical Technique for Food Quality and Safety Monitoring. *Food Biosci.* **2023**, *56*, 103392.
(9) Findlay, C. R.; Wiens, R.; Rak, M.; Sedlmair, J.; Hirschmugl, C. J.; Morrison, J.; Mundy, C. J.; Kansiz, M.; Gough, K. M. Rapid Biodiagnostic Ex Vivo Imaging at 1 Mm Pixel Resolution with Thermal Source FTIR FPA. *Analyst* **2015**, *140* (7), 2493−2503.
(10) Zhang, J.; Liu, L.; Jiang, Y.; Faisal, S.; Wei, L.; Cao, C.; Yan, W.; Wang, Q. Converting Peanut Protein Biomass Waste into "Double Green" Meat Substitutes Using a High-Moisture Extrusion Process: A Multiscale Method to Explore a Process for Forming a Meat-Like Fibrous Structure. *J. Agric. Food Chem.* **2019**, *67* (38), 10713−10725.
(11) Ghanghas, N.; Nadimi, M.; Paliwal, J.; Koksel, F. Gas-Assisted High-Moisture Extrusion of Soy-Based Meat Analogues: Impacts of Nitrogen Pressure and Cooling Die Temperature on Density, Texture and Microstructure. *Innovative Food Sci. Emerging Technol.* **2024**, *92*, 103557.
(12) Elhordoy, M. R.; Kadam, A.; Vazquez, D.; Medrano, A.; Koksel, F. Exploring the Potential of Lupin (Lupinus Angustifolius) Flour-Based Ingredients in Developing High Moisture Meat Analogues. *J. Food Sci.* **2025**, *90* (7), No. e70407.
(13) Singh, R.; Sá, A. G. A.; Sharma, S.; Nadimi, M.; Paliwal, J.; House, J. D.; Koksel, F. Effects of Feed Moisture Content on the Physical and Nutritional Quality Attributes of Sunflower Meal-Based High-Moisture Meat Analogues. *Food Bioprocess Technol.* **2024**, *17*, 1897.
(14) Singh, A.; Tulbek, N. C.; Izydorczyk, M.; Koksel, F. High Moisture Extrusion Texturization of Air-Classified Barley Protein for the Production of Novel Plant-Based Meat Analogues. *Food Bioprocess Technol.* **2025**, *18*, 1857−1872.
(15) Baker, M. J.; Trevisan, J.; Bassan, P.; Bhargava, R.; Butler, H. J.; Dorling, K. M.; Fielden, P. R.; Fogarty, S. W.; Fullwood, N. J.; Heys, K. A.; et al. Using Fourier Transform IR Spectroscopy to Analyze Biological Materials. *Nat. Protoc.* **2014**, *9* (8), 1771−1791.
(16) Bakir, G.; Girouard, B. E.; Wiens, R.; Mastel, S.; Dillon, E.; Kansiz, M.; Gough, K. M. Orientation Matters: Polarization Dependent IR Spectroscopy of Collagen from Intact Tendon Down to the Single Fibril Level. *Molecules* **2020**, *25* (18), 4295.
(17) Bakir, G.; Dahms, T. E. S.; Martin-Yken, H.; Bechtel, H. A.; Gough, K. M. Saccharomyces Cerevisiae CellWall Remodeling in the Absence of Knr4 and Kre6 Revealed by Nano-FourierTransform Infrared Spectroscopy. *Appl. Spectrosc.* **2024**, *78* (4), 355−364.
(18) Krimm, S.; Bandekar, J. Vibrational Spectroscopy and Conformation of Peptides, Polypeptides, and Proteins. In *Advances in Protein Chemistry*; Anfinsen, C. B., Edsall, J. T., Richards, F. M., Eds.; Academic Press, 1986; Vol. *38*, pp 181−364.10.1016/S0065-3233(08)60528-8.
(19) Denavi, G. A.; Pérez-Mateos, M.; Añón, M. C.; Montero, P.; Mauri, A. N.; Gómez-Guillén, M. C. Structural and Functional Properties of Soy Protein Isolate and Cod Gelatin Blend Films. *Food Hydrocolloids* **2009**, *23* (8), 2094−2101.
(20) Petersen, M. T. N.; Jonson, P. H.; Petersen, S. B. Amino Acid Neighbours and Detailed Conformational Analysis of Cysteines in Proteins. *Protein Eng.* **1999**, *12* (7), 535−548.
(21) Shrestha, S.; van't Hag, L.; Haritos, V. S.; Dhital, S. Lupin Proteins: Structure, Isolation and Application. *Trends Food Sci. Technol.* **2021**, *116*, 928−939.
(22) Devkota, L.; Kyriakopoulou, K.; Bergia, R.; Dhital, S. Structural and Thermal Characterization of Protein Isolates from Australian Lupin Varieties as Affected by Processing Conditions. *Foods* **2023**, *12* (5), 908.
(23) Bouyanfif, A.; Liyanage, S.; Hequet, E.; Moustaid-Moussa, N.; Abidi, N. FTIR Microspectroscopy Reveals Fatty Acid-Induced Biochemical Changes in *C. Elegans*. *Vib. Spectrosc.* **2019**, *102*, 8−15.
(24) Stitt, D. M.; Kastyak-Ibrahim, M. Z.; Liao, C. R.; Morrison, J.; Albensi, B. C.; Gough, K. M. Tissue Acquisition and Storage Associated Oxidation Considerations for FTIR Microspectroscopic Imaging of Polyunsaturated Fatty Acids. *Vib. Spectrosc.* **2012**, *60*, 16−22.
(25) Johnson, S. K.; Clements, J.; Villarino, C. B. J.; Coorey, R. Lupins: Their Unique Nutritional and Health-Promoting Attributes. In *Gluten-Free Ancient Grains*; Taylor, J. R. N., Awika, J. M., Eds.; Woodhead Publishing Series in Food Science, Technology and Nutrition; Woodhead Publishing, 2017; Chapter 8, pp 179−221.10.1016/B978-0-08-100866-9.00008-X.
(26) Smith, B. C. An IR Spectral Interpretation Potpourri: Carbohydrates and Alkynes. *Spectroscopy* **2017**, *32* (7), 18−24.
(27) Hong, T.; Yin, J.-Y.; Nie, S.-P.; Xie, M.-Y. Applications of Infrared Spectroscopy in Polysaccharide Structural Analysis: Progress, Challenge and Perspective. *Food Chem.:X* **2021**, *12*, 100168.
(28) Wathoni, N.; Yuan Shan, C.; Yi Shan, W.; Rostinawati, T.; Indradi, R. B.; Pratiwi, R.; Muchtaridi, M. Characterization and Antioxidant Activity of Pectin from Indonesian Mangosteen (*Garcinia Mangostana* L.) Rind. *Heliyon* **2019**, *5* (8), No. e02299.

(29) Malekipoor, R.; Johnson, S. K.; Bhattarai, R. R. Lupin Kernel Fibre: Nutritional Composition, Processing Methods, Physicochemical Properties, Consumer Acceptability and Health Effects of Its Enriched Products. *Nutrients* **2022**, *14* (14), 2845.
(30) Mohamed, A. A.; Rayas-Duarte, P. Nonstarchy Polysaccharide Analysis of Cotyledon and Hull of Lupinus Albus. *Cereal Chem.* **1995**, *72* (6), 648−651.
(31) van der Sman, R. G. M.; van der Goot, A. J. Hypotheses Concerning Structuring of Extruded Meat Analogs. *Curr. Res. Food Sci.* **2023**, *6*, 100510.
(32) Schmid, E. M.; Farahnaky, A.; Adhikari, B.; Torley, P. J. High Moisture Extrusion Cooking of Meat Analogs: A Review of Mechanisms of Protein Texturization. *Compr. Rev. Food Sci. Food Saf.* **2022**, *21* (6), 4573−4609.
(33) Ozturk, O. K.; Hamaker, B. R. Texturization of Plant Protein-Based Meat Alternatives: Processing, Base Proteins, and Other Constructional Ingredients. *Future Foods* **2023**, *8*, 100248.
(34) Zhang, Z.; Zhang, L.; He, S.; Li, X.; Jin, R.; Liu, Q.; Chen, S.; Sun, H. High-Moisture Extrusion Technology Application in the Processing of Textured Plant Protein Meat Analogues: A Review. *Food Rev. Int.* **2023**, *39* (8), 4873−4908.
(35) Dinali, M.; Liyanage, R.; Silva, M.; Newman, L.; Adhikari, B.; Wijesekara, I.; Chandrapala, J. Fibrous Structure in Plant-Based Meat: High-Moisture Extrusion Factors and Sensory Attributes in Production and Storage. *Food Rev. Int.* **2024**, *40* (9), 2940−2968.
(36) Sandoval Murillo, J. L.; Osen, R.; Hiermaier, S.; Ganzenmüller, G. Towards Understanding the Mechanism of Fibrous Texture Formation during High-Moisture Extrusion of Meat Substitutes. *J. Food Eng.* **2019**, *242*, 8−20.
(37) Liu, K. S.; Hsieh, F. H. Protein-Protein Interactions during High-Moisture Extrusion for Fibrous Meat Analogues and Comparison of Protein Solubility Methods Using Different Solvent Systems. *J. Agric. Food Chem.* **2008**, *56* (8), 2681−2687.
(38) Wang, S.; Chao, C.; Cai, J.; Niu, B.; Copeland, L.; Wang, S. Starch−Lipid and Starch−Lipid−Protein Complexes: A Comprehensive Review. *Compr. Rev. Food Sci. Food Saf.* **2020**, *19* (3), 1056−1079.
(39) Putseys, J. A.; Lamberts, L.; Delcour, J. A. Amylose-Inclusion Complexes: Formation, Identity and Physico-Chemical Properties. *J. Cereal Sci.* **2010**, *51* (3), 238−247.
(40) Godet, M. C.; Bizot, H.; Buléon, A. Crystallization of Amylose—Fatty Acid Complexes Prepared with Different Amylose Chain Lengths. *Carbohydr. Polym.* **1995**, *27* (1), 47−52.
(41) Li, X.; Wang, C.; Chao, C.; Yu, J.; Copeland, L.; Liu, Y.; Wang, S. Prior Interaction of Protein and Lipid Affects the Formation of Ternary Complexes with Starch. *Food Chem.* **2023**, *426*, 136500.
(42) Chao, C.; Cai, J.; Yu, J.; Copeland, L.; Wang, S.; Wang, S. Toward a Better Understanding of Starch−Monoglyceride−Protein Interactions. *J. Agric. Food Chem.* **2018**, *66* (50), 13253−13259.
(43) Zhang, G.; Maladen, M. D.; Hamaker, B. R. Detection of a Novel Three Component Complex Consisting of Starch, Protein, and Free Fatty Acids. *J. Agric. Food Chem.* **2003**, *51* (9), 2801−2805.
(44) Zhang, G.; Hamaker, B. R. A Three Component Interaction among Starch, Protein, and Free Fatty Acids Revealed by Pasting Profiles. *J. Agric. Food Chem.* **2003**, *51* (9), 2797−2800.
(45) Luo, S.; Koksel, F. Real-Time Thermal Imaging of Expansion Dynamics during Extrusion of Protein-Fortified Snacks: Effects of Nitrogen Gas and Protein Concentration. *Food Res. Int.* **2025**, *199*, 115349.
(46) Wang, S.; Chao, C.; Xiang, F.; Zhang, X.; Wang, S.; Copeland, L. New Insights into Gelatinization Mechanisms of Cereal Endosperm Starches. *Sci. Rep.* **2018**, *8* (1), 3011.
(47) Dominguez-Ayala, J. E.; Ayala-Ayala, M. T.; Velazquez, G.; Espinosa-Arbelaez, D. G.; Mendez-Montealvo, G. Crystal Structure Changes of Native and Retrograded Starches Modified by High Hydrostatic Pressure: Physical Dual Modification. *Food Hydrocolloids* **2023**, *140*, 108630.
(48) Enríquez-Castro, C. M.; Ramírez-Wong, B.; Contreras-Jiménez, B. L.; Quintero-Ramos, A.; de Dios Figueroa-Cárdenas, J.; Vázquez-Lara, F. Effect of Extrusion on the Crystallinity, Viscosity, Damage Starch, and Thermal Properties of Corn Flour, Masa, and Tortilla. *Appl. Food Res.* **2022**, *2* (2), 100198.
(49) Gamarano, D. d. S.; Pereira, I. M.; da Silva, M. C.; Mottin, A. C.; Ayres, E. Crystal Structure Transformations in Extruded Starch Plasticized with Glycerol and Urea. *Polym. Bull.* **2020**, *77* (9), 4971−4992.
(50) Rodriguez-Garcia, M. E.; Hernandez-Landaverde, M. A.; Delgado, J. M.; Ramirez-Gutierrez, C. F.; Ramirez-Cardona, M.; Millan-Malo, B. M.; Londoño-Restrepo, S. M. Crystalline Structures of the Main Components of Starch. *Curr. Opin. Food Sci.* **2021**, *37*, 107−111.
(51) Singh, J.; Kaur, L.; McCarthy, O. J. Factors Influencing the Physico-Chemical, Morphological, Thermal and Rheological Properties of Some Chemically Modified Starches for Food Applications—A Review. *Food Hydrocolloids* **2007**, *21* (1), 1−22.
(52) Ma, C.-Y.; Rout, M. K.; Mock, W.-Y. Study of Oat Globulin Conformation by Fourier Transform Infrared Spectroscopy. *J. Agric. Food Chem.* **2001**, *49* (7), 3328−3334.
(53) Devi, T. A.; Rahul, R.; Joshua, H. M.; Naveen, N.; Karthik, P. Formulation of Plant-Based Meat Alternatives and Its Optimization by Experimental Design Using Response Surface Methodology. *Sustainable Food Technol.* **2024**, *2* (4), 1139−1151.
(54) Candoğan, K.; Altuntas, E. G.; İğci, N. Authentication and Quality Assessment of Meat Products by Fourier-Transform Infrared (FTIR) Spectroscopy. *Food Eng. Rev.* **2021**, *13* (1), 66−91.
(55) Garip, S.; Gozen, A. C.; Severcan, F. Use of Fourier Transform Infrared Spectroscopy for Rapid Comparative Analysis of *Bacillus* and *Micrococcus* Isolates. *Food Chem.* **2009**, *113* (4), 1301−1307.
(56) Xia, S.; Song, J.; Li, K.; Hao, T.; Ma, C.; Shen, S.; Jiang, X.; Xue, C.; Xue, Y. Yeast Protein-Based Meat Analogues: Konjac Glucomannan Induces the Fibrous Structure Formation by Modifying Protein Structure. *Food Hydrocolloids* **2023**, *142*, 108798.
(57) Bhuiyan, M. H. R.; Liu, L.; Samaranayaka, A.; Ngadi, M. Prediction of Pea Composites Physicochemical Traits and Techno-functionalities using FTIR Spectroscopy. *LWT* **2024**, *208*, 116667.

https://doi.org/10.1021/acs.jafc.5c10733
J. Agric. Food Chem. 2026, 74, 5616−5626